ATLAS NOTE

ATLAS-CONF-2013-084

August 11, 2013

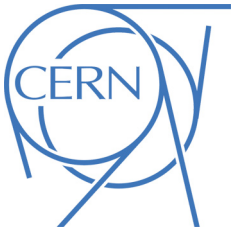

Performance of boosted top quark identification in 2012 ATLAS data

The ATLAS Collaboration

Abstract

This note presents the performance of a variety of techniques used to identify highly-boosted top quarks. The studies presented here use the full 2012 ATLAS dataset taken at a center of mass energy of $\sqrt{s}$ = 8 TeV, corresponding to an integrated luminosity of (20.3±0.6) fb^{-1} of proton–proton collisions produced by the Large Hadron Collider. A sample enriched in $t\bar{t} \to (Wb)(Wb) \to (qqb)(\mu\nu b)$ events is used for the study. Following the jet trimming procedure, large-R jet substructure properties are shown to be well described by the simulation. Additionally, the distribution of subjets from the trimming process is used to characterize events in which the hadronic daughter particles of a boosted top quark are fully contained within the distance parameter of a large-R jet. Performance of top quark mass reconstruction using the HEPTopTagger algorithm is also shown and demonstrates an insensitivity to additional proton–proton interactions per event. The distributions of the tagger internal substructure variables and the tagged jet mass are well described by the simulation. Various working points of different tagging approaches are compared in simulation between a signal of large-R jets containing highly boosted top quarks and a background of large-R jets originating from hard light quarks or gluons. In addition to the HEPTopTagger, which gives a high rejection of background jets and a medium top quark jet tagging efficiency of 30–40% depending on the algorithm parameters, several taggers that are based on selecting on substructure variables are studied and shown to yield higher efficiencies at reduced rejection.

ATLAS-CONF-2013-084
11 August 2013

1 Introduction

With proton-proton (pp) collisions provided by the Large Hadron Collider (LHC) at $\sqrt{s} = 8$ TeV, over one thousand Standard Model (SM) $t\bar{t}$ events per fb^{-1} are expected with hadronic top transverse momentum p_{T} greater than 300 GeV.[1] New physics may appear in this region of phase space, the study of which was limited by integrated luminosity and available energy at previous colliders.

When sufficiently boosted, the decay products of a top quark can become collimated to the point that standard top reconstruction techniques begin to fail. In the case where a highly boosted top quark decays into a b-quark and a hadronically decaying W boson, the separation of the three daughter quarks can become smaller than the distance parameter of the jets, often failing to be individually resolved by standard jet algorithms. Moreover, the high-luminosity conditions at the LHC can further degrade the procedures for reconstructing decays of boosted top quarks. Multiple pp interactions per bunch crossing (pile-up) produce soft particles unrelated to the hard scattering that can contaminate jets in the detector considerably more than at previous hadron-hadron colliders. In events where the three daughter quarks are fully contained within an individual large-distance-parameter (large-R) jet, a diminished jet mass resolution due to pile-up may dramatically weaken sensitivity to new physics processes.

Because a single jet that contains all of the decay products of a massive particle has significantly different properties than a jet of the same momentum originating from a light quark or gluon, it is possible to use the substructure of a large-R jet to distinguish boosted top quarks from a large multi-jet background. These subtle differences in substructure can be resolved more clearly after removing soft QCD radiation and pileup contributions from jets. Such adaptive modification of the jet algorithm or selective removal of soft radiation during the process of iterative recombination in jet reconstruction is generally referred to as *jet grooming* [1–3].

The note is organized as follows. Section 2 introduces the jet grooming and substructure techniques studied in this note and also gives a description of the HEPTopTagger [4, 5], a boosted top-tagging algorithm. Section 3 describes the ATLAS detector, the 2012 dataset and simulation samples, and the selection used to identify $t\bar{t}$ events. Section 4 shows the modeling of data by the simulation for boosted top quarks contained in large-R groomed jets in various p_{T}-regimes. Section 5 describes the calibration of the HEPTopTagger algorithm and the performance of the tagger in data. Finally, Section 6 compares the top-tagging efficiency and background rejection in simulation for various HEPTopTagger tunes and groomed jet substructure selections using a signal sample of boosted top quarks and a background sample of light quarks and gluons.

2 Jet reconstruction, grooming and substructure

The standard inputs to jet reconstruction in ATLAS are massless topological clusters of calorimeter cell energy depositions [6], where only clusters with positive energy after noise correction are considered. Depending on the cluster energy density, likelihoods are calculated that the cluster results from electromagnetic or hadronic interactions and a correction is applied to the cluster energy based on simulations of single pion interactions with the calorimeter (a process known as local cluster weighting, or LCW). Truth-level particle jets, built from generated stable particles from the event generator, are used to calibrate the calorimeter response.

[1] The ATLAS coordinate system is a right-handed system with the x-axis pointing to the center of the LHC ring and the y-axis pointing upwards. The polar angle θ is measured with respect to the LHC beam-line. The azimuthal angle ϕ is measured with respect to the x-axis. The rapidity is defined as $y = 0.5 \times \ln[(E + p_z)/(E - p_z)]$, where E denotes the energy and p_z is the component of the momentum along the beam direction. The pseudorapidity η is an approximation for rapidity y in the high-energy limit, and it is related to the polar angle θ by $\eta = -\ln\tan(\theta/2)$. Transverse momentum and energy are defined as $p_{\mathrm{T}} = p \times \sin\theta$ and $E_{\mathrm{T}} = E \times \sin\theta$, respectively.

In this note, three jet-reconstruction algorithms are used: the k_t [7–9], the Cambridge–Aachen (C/A) [10, 11], and the anti-k_t [12] algorithms. These are implemented within the framework of the FastJet software [13, 14]. The clustering histories of the k_t and C/A algorithms – that is, the ordering and structure of the pair-wise subjet 4-vector recombinations made during jet reconstruction – provide spatial and kinematic information about the substructure of a jet, while the anti-k_t algorithm provides jets that are defined primarily by the highest-p_{T} constituent, yielding relatively circular jets.

Previous studies of boosted top quark identification using jet substructure with the 2011 ATLAS dataset taken at $\sqrt{s} = 7$ TeV can be found in Ref. [15], which also contains detailed descriptions of the algorithms and extensive studies on the optimization of grooming algorithms for ATLAS boosted top analyses. The techniques used in the studies presented here are:

- *Jet trimming* - The trimming algorithm [3] has been adopted by ATLAS as the standard grooming procedure for boosted top analyses using the anti-k_t ($R = 1.0$) jet algorithm. It uses a k_t algorithm to create subjets with $R_{\mathrm{sub}} = 0.3$ from the constituents of a jet with transverse momentum $p_{\mathrm{T}}^{\mathrm{jet}}$. Any subjets with $p_{\mathrm{T}i}/p_{\mathrm{T}}^{\mathrm{jet}} < f_{\mathrm{cut}}$ are removed, where $p_{\mathrm{T}i}$ is the transverse momentum of the i^{th} subjet, and f_{cut} is a parameter of the procedure set to 5% for the studies in this note. The remaining constituents form the trimmed jet. Because this procedure discards the softer components of the jet, contributions from pile-up and the underlying event are preferentially removed.

- *k_t splitting scales* - The k_t splitting scales are determined by reclustering the constituents of a jet with the k_t algorithm, which tends to combine the harder constituents last. A k_t distance measure between the last combined subjets can be used to define a splitting scale variable as:

$$\sqrt{d_{ij}} = \min(p_{\mathrm{T}i}, p_{\mathrm{T}j}) \times \Delta R_{ij}, \tag{1}$$

  where ΔR_{ij} is the distance between the two subjets in $\eta - \phi$ space. Subjets identified at the last step of the reclustering in the k_t algorithm provide the $\sqrt{d_{12}}$ observable, and $\sqrt{d_{23}}$ characterizes the splitting scale in the second-to-last step of the reclustering.

- *N-subjettiness* - The N-subjettiness variables τ_N [16, 17] describe how well jets can be described as containing N or fewer k_t subjets. The N subjets found by an exclusive clustering of the constituents of a jet with the k_t algorithm [9] define axes within the jet. The τ_N variables are given by the sum over all constituents k of the jet, such that

$$\tau_N = \frac{1}{d_0} \sum_k p_{\mathrm{T}k} \times \min(\Delta R_{1k}, \Delta R_{2k}, ..., \Delta R_{Nk}) \,, \text{ with } \; d_0 \equiv \sum_k p_{\mathrm{T}k} \times R \tag{2}$$

  where R is the jet distance parameter in the jet algorithm, $p_{\mathrm{T}k}$ is the p_{T} of constituent k and ΔR_{ik} is the distance from subjet i to constituent k. The ratios τ_2/τ_1 (denoted τ_{21}) and τ_3/τ_2 (denoted τ_{32}) can be used to provide discrimination between jets formed from boosted top quarks and those produced from light quarks or gluons.

- *HEPTopTagger* - The HEPTopTagger algorithm [4, 5] identifies the hard substructure of a C/A $R = 1.5$ jet and tests it for compatibility with the 3-prong pattern of hadronic top quark decay. The tagger has been developed to find mildly boosted top quarks with $p_{\mathrm{T}} > 200$ GeV in events with an associated production of top quarks with a Higgs boson. The algorithm uses internal parameters that can be changed to optimize the performance. The tagger uses three main steps. In the first step, the massive C/A jet is iteratively broken down into hard substructure objects using a mass drop criterion as described in Ref. [1]. The procedure stops when all substructure objects have a mass below the value m_{cut}. In the second phase, all combinations of three substructure

objects are tested for compatibility with hadronic top quark decay. Energy contributions from underlying event and pile-up are removed using a filtering procedure that adapts to the distance of the substructure objects. Small distance parameter C/A jets are built from the constituents of the substructure objects using a value of R_{filt} that depends on the distance between these objects. A maximum $R_{\text{filt}}^{\text{max}}$ can be set. The constituents of the N_{filt} largest p_{T} filter jets are then clustered into three top quark subjets using the exclusive C/A algorithm. In the last step, kinematic cuts are applied to differentiate top quark decays from background. One of the criteria is that one pair of subjets must have an invariant mass that falls inside a W boson mass window, the width of which is given by f_W. If all criteria are met, the large-R jet is considered to be tagged. The top quark candidate four-momentum vector is given by the sum of the vectors of the N_{filt} largest p_{T} filter jets. The parameter settings used in this note are summarized in Table 1. The parameters listed in the 'default value' column gave the best expected significance in a search for fully hadronic $t\bar{t}$ resonances with 2011 data [18].

parameter	description	default value	tight	loose
m_{cut}	maximum mass of substructure objects	50 GeV	30 GeV	70 GeV
$R_{\text{filt}}^{\text{max}}$	maximum filtering subjet distance parameter	0.3	0.2	0.5
N_{filt}	number of filtering subjets used	5	4	7
f_W	width of W boson mass window	±15%	±10%	±20%

Table 1: The HEPTopTagger parameter settings used in this note.

3 The ATLAS Detector, data and simulation samples and event selection

3.1 Data quality criteria and event selection

The studies presented in this note are based on the 2012 dataset recorded by the ATLAS experiment [19], corresponding to an integrated luminosity of 20.3 fb^{-1}. The uncertainty on the integrated luminosity is ±2.8%. It is derived from a preliminary calibration of the luminosity scale derived from beam-separation scans performed in November 2012, following the methodology detailed in Ref. [20].

Data-taking periods in which the detector was fully functional are used, and the data are required to meet baseline quality criteria. These criteria reject significant contamination from detector noise, non-collision beam backgrounds, and other spurious effects. The ATLAS data quality selection is based upon individual assessments for each subdetector, usually separated into barrel, endcap and forward regions, as well as for the trigger and for each type of reconstructed physics object (jets, muons, etc.).

3.2 Monte Carlo simulation

A sample of $t\bar{t}$ events filtered for a lepton (at least one electron, muon or tau in the final state) are produced with the POWHEG-BOX 1.0 [21–23] generator using the CT10 NLO PDF set [24] in the matrix element. This is interfaced to PYTHIA 6.425 [25] for the hadronization and underlying event models using the CTEQ6L1 PDF set [26] and the Perugia 2011C tune [27, 28].

Additionally, several samples simulating the background to boosted $t\bar{t}$ events are produced. Single-top-quark events in the s-channel final state $t + j$, where the W bosons in the final state produced from the top quark are required to decay leptonically, are generated with MC@NLO [29, 30] using the CT10 NLO PDF [24] set. Final-state parton showers are simulated and hadronized using the HERWIG 6.520.2 [31] program interfaced to the JIMMY 4.31.3 underlying event model [32] with the ATLAS AUET2 tune [27,

28]. Events produced in the Wt channel, where all non-top originating W boson decay channels are produced, are also generated with MC@NLO and the same parton shower, PDF and tune as for the $t + j$ s-channel. Events in the single top t-channel are generated with AcerMC [33] using the CTEQ6L1 PDF set, and are showered using PYTHIA 6.425 with the AUET2B tune [34]. Samples of W+jets and Z+jets events are produced with the ALPGEN 2.14 [35] generator, using CTEQ6L1 PDFs, interfaced to PYTHIA 6.425 using the Perugia 2011C tune for parton showering and hadronization. A scale factor of 0.8 applied to the normalization of the W+jets simulation sample has been determined from data using the lepton charge asymmetry in $t\bar{t}$ events [36, 37].

To study the boosted top quark tagging performance with high-p_{T} top quarks, a $Z' \rightarrow t\bar{t}$ sample is produced using PYTHIA 8.160 [38] with the MSTW2008 LO PDF [39] and the ATLAS AU2 tune [34]. The rejection of background by the top tagging algorithms is studied using a dijet sample generated with PYTHIA 8.160 using the CT10 LO PDF and the AU2 tune.

Additional pile-up interactions in each simulated event are modeled by adding multiple soft pp collisions generated by PYTHIA 8.165 with the MSTW2008 LO PDF and A2 tune [34]. After event generation and the addition of pile-up, the response of the ATLAS detector to particles passing through the detector elements is simulated with the GEANT4 toolkit [40, 41] and events are reconstructed using the same software used to reconstruct events in data.

3.3 Selection of events with boosted top quark decays

The performance of top quark identification is studied using a sample that is enriched in $t\bar{t}$ events. The semileptonic $t\bar{t}$ decay mode in which one W boson decays into a neutrino and a muon is chosen to reduce the multi-jet background, thus making the top quark signal discernible.

To reject non-collision beam backgrounds, events are required to contain at least two reconstructed primary vertices, each with at least two tracks associated to them. Additionally, all anti-k_t $R = 0.4$ jets with $p_{\mathrm{T}}^{\mathrm{jet}} > 20$ GeV and $|\eta^{\mathrm{jet}}| < 2.5$ are required to satisfy the "looser" quality criteria discussed in detail in Ref. [42]. Any event containing a jet of this type that fails the "looser" selection criterion is rejected.

The events are required to pass either of two muon triggers in the online event filter, where one is optimized to select isolated muons with a transverse momentum of at least 24 GeV and the other selects muons with at least 36 GeV without the isolation requirement. Exactly one muon is required that must be reconstructed in both the inner detector and the muon spectrometer with $p_{\mathrm{T}} > 25$ GeV and $|\eta| < 2.5$. The longitudinal impact parameter with respect to the primary vertex having the highest $\sum p_{\mathrm{T}}^2$ of constituent tracks is required to be smaller than 2 mm. The muon is required to be isolated by requiring the ratio of the summed transverse track momentum within a cone of size $\Delta R = 10$ GeV$/p_{\mathrm{T}}^{\mu}$ around the muon track to be less than 5% of the muon transverse momentum p_{T}^{μ}.

To select events with a leptonically decaying W boson, events are required to have missing transverse momentum $E_{\mathrm{T}}^{\mathrm{miss}} > 20$ GeV. Additionally, the scalar sum of $E_{\mathrm{T}}^{\mathrm{miss}}$ and the transverse mass of the leptonic W boson candidate must have $E_{\mathrm{T}}^{\mathrm{miss}} + m_{\mathrm{T}}^{W} > 60$ GeV, where $m_{\mathrm{T}}^{W} = \sqrt{2p_{\mathrm{T}}^{\mu}E_{\mathrm{T}}^{\mathrm{miss}}(1 - \cos\Delta\phi)}$ is calculated from the muon p_{T} and the $E_{\mathrm{T}}^{\mathrm{miss}}$ in the event, and $\Delta\phi$ is the azimuthal angle between the muon candidate and the $E_{\mathrm{T}}^{\mathrm{miss}}$.

To reduce contamination from W+jets events, each event must contain at least one b-tagged anti-k_t jet with $R = 0.4$ having $p_{\mathrm{T}}^{\mathrm{jet}} > 20$ GeV and $|\eta^{\mathrm{jet}}| < 2.5$. The standard ATLAS b-tagging algorithm is a neural-network-based tagger [43] that uses information on the impact parameters, the secondary vertex and the decay topology as its input. The algorithm operating point chosen for this analysis corresponds to a b-tagging identification efficiency of 70%. At least one of these b-tagged jets is required to be within $\Delta R = 1.5$ of the muon. This loose muon association has a high $t\bar{t}$ signal efficiency while greatly reducing the large W+jets background.

The events are also required to contain a high-p_{T} large-R jet to select topologies in which the hadronic

top quark decay products are collimated. To study the performance of jet trimming, at least one trimmed anti-k_t $R = 1.0$ jet with $p_{\mathrm{T}} > 200$ GeV is required. The trimmed large-R jet is calibrated using a MC-based calibration scheme as described in Ref. [15]. For the HEPTopTagger, which is optimized to find top quarks with low transverse momentum, each event has to contain at least one $R = 1.5$ C/A jet with $p_{\mathrm{T}} > 200$ GeV.

According to simulation, 79% of the events with a $R = 1.5$ C/A jet after selection contain $t\bar{t}$ pairs in which one of the top quarks decays (via a W boson) into a muon and corresponding neutrino, and the second top quark decays hadronically. The remaining events are dominated by W+jets production, with small contributions from Z+jets and single-top-quark processes.

4 Large-R jet trimming with boosted tops

4.1 Boosted tops in data

Comparisons between the full 2012 dataset and simulation are made for the leading p_{T} trimmed anti-k_t jet with $R = 1.0$. After the selection described in Section 3.3, a deficit in MC compared to data as a function of the leading jet p_{T} is observed. This can be seen in Figure 1, where the data is overestimated by the simulation in events with leading jet $p_{\mathrm{T}} > 400$ GeV. There are large theoretical uncertainties associated with the modeling of this jet p_{T} spectrum, and thus no attempt is made to correct the distribution from the MC simulation in this study.

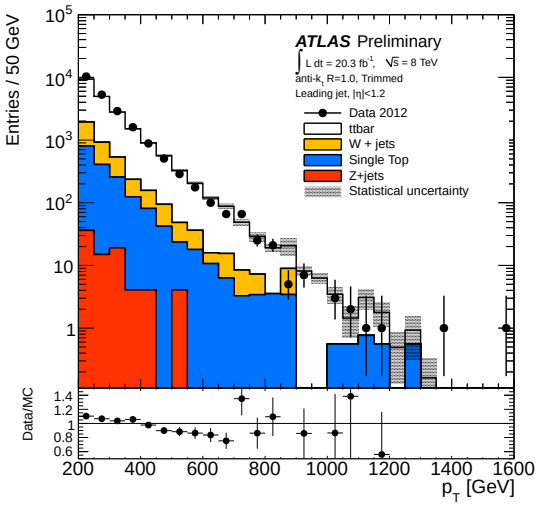

Figure 1: Leading-p_{T} jet p_{T} spectrum for anti-k_t trimmed jets with $R = 1.0$ and $|\eta| < 1.2$. The shaded band represents the bin-by-bin statistical uncertainty in simulation.

When considering the performance of trimming for jets with mass m^{jet} around m_t (the top quark mass), it is important to distinguish $t\bar{t}$ events in which it is geometrically possible to form a large-R jet containing all the daughter particles of a hadronically decaying top quark from those where it is not, due to one of the decay products falling outside the jet. The $t\bar{t}$ simulation is divided into two categories, "non-contained" and "contained", where the latter refers to events in which each of the daughter particles $q_i \in \{b,\ q,\ q\}$ of the hadronically decaying top (or anti-top) quark t at the truth level before radiation must be within a separation $\Delta R(q_i, t) < 1.0$ from the true parent top quark direction. There is no matching of the truth top direction to the leading-p_{T} jet. "Non-contained" refers to the remaining events in the $t\bar{t}$ simulation where it is not expected to have all decay products within the area of an anti-k_t jet with

$R = 1.0$. This category also includes $t\bar{t}$ events in which both W bosons decay leptonically, or where the W decayed into an electron or tau with corresponding neutrino, but these contributions are small.

Figure 2 shows the jet mass for trimmed jets with $p_{\mathrm{T}} > 350$ GeV (a) and $p_{\mathrm{T}} > 500$ GeV (b). The main non-top quark background, W+jets, exhibits a steeply falling jet mass spectrum, while the boosted top is clearly visible around $m^{\mathrm{jet}} \approx m_t$. There are also peaks at low mass and near $m^{\mathrm{jet}} \approx m_W$ (the W boson mass), where only one or two decay product(s) are contained within the jet, respectively (this shall be discussed in more detail in Section 4.2). The shape of the mass distribution near m_t is well modeled in simulation, with a slight underestimation of the number of events compared to data around m_W.

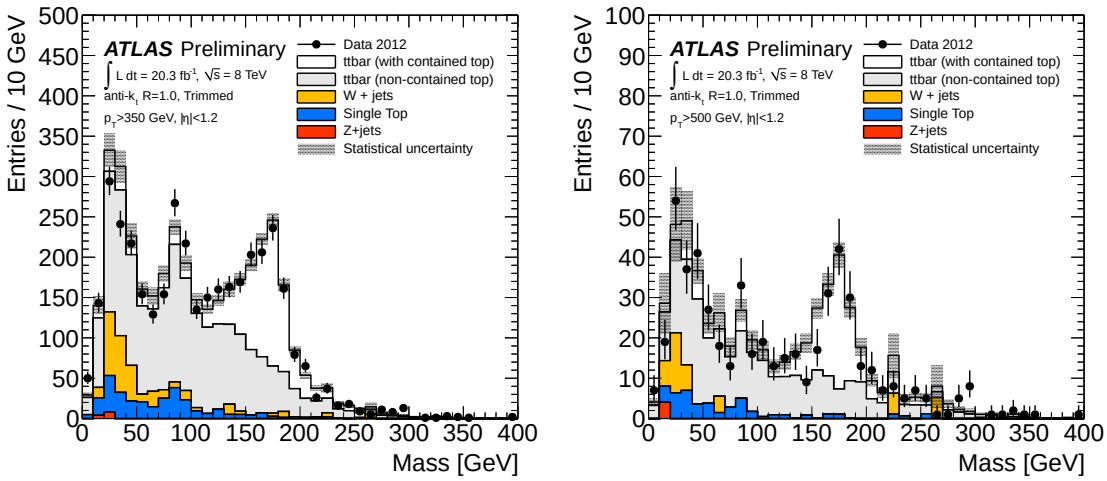

(a) $p_{\mathrm{T}} > 350$ GeV

(b) $p_{\mathrm{T}} > 500$ GeV

Figure 2: Jet mass for leading p_{T} anti-k_t trimmed jets with $R = 1.0$, $|\eta| < 1.2$ and two jet p_{T} thresholds. Here, "contained" refers to events having a hadronically-decaying top quark with collimated daughter particles at the truth level (all three daughter quarks q_i satisfy $\Delta R(q_i, t)$ <1.0). The shaded band represents the bin-by-bin statistical uncertainty in simulation.

The parameters chosen for the trimming algorithm were determined partly for the resilience of the trimmed jet mass to the effects of pile-up. Figure 3 shows the average mass of the leading p_{T} trimmed anti-k_t $R = 1.0$ jet with $p_{\mathrm{T}} > 350$ GeV and $|\eta| < 1.2$ after the b-tagging requirement versus the average number of inelastic pp collisions per bunch crossing, $\langle\mu\rangle$, which is calculated from the instantaneous luminosity and LHC beam parameters, as well as versus the total number of primary vertices measured in the event, N_{PV}. Due to other non-$t\bar{t}$ background events at low mass, jets in these figures are required to have $m^{\mathrm{jet}} > 100$ GeV.

Figure 4 shows the simulation compared to data after a b-tagging requirement for the parameters $\sqrt{d_{12}}$ and $\sqrt{d_{23}}$. The splitting scales tend to be reasonably symmetric when the decay is to like-mass particles, as opposed to the largely asymmetric splittings that originate from QCD radiation in light-quark or gluon jets. The expected value of the first splitting scale for a "contained" boosted top quark is approximately $\sqrt{d_{12}} \approx m_t/2$, whereas jets from the parton shower of gluons and light quarks tend to have smaller values of the splitting scales and to exhibit a steeply falling spectrum. The second splitting scale, $\sqrt{d_{23}}$, also provides discrimination from the three-body decay of the contained boosted top quark compared to a light-quark or gluon jet background, as it targets the splitting of the W boson with an expected value of $\sqrt{d_{23}} \approx m_W/2$.

In Figure 5, the N-subjettiness variables τ_1, τ_2 and τ_3 as well as the ratios τ_{21} and τ_{32} are shown

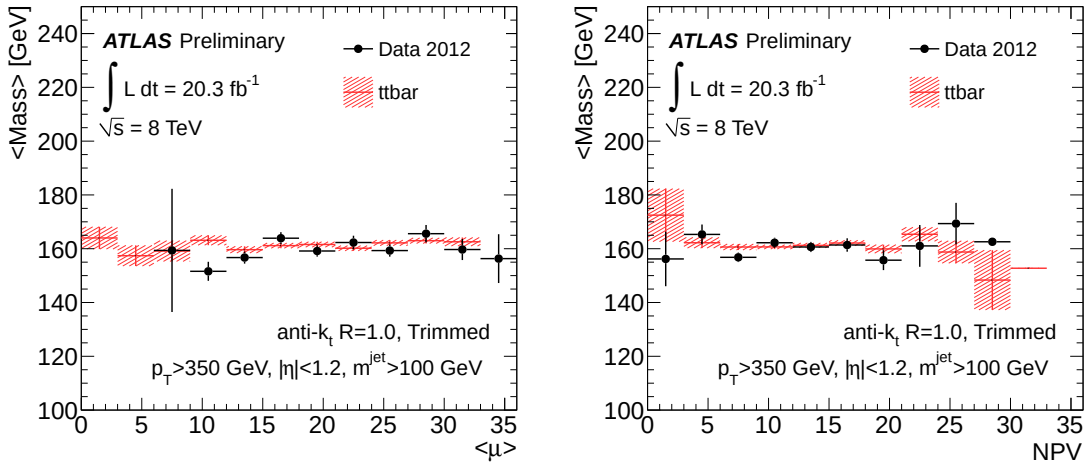

(a) (b)

Figure 3: Average mass for leading p_{T} anti-k_t trimmed jets with $R = 1.0$, $p_{\mathrm{T}} > 350$ GeV, $|\eta| < 1.2$ and $m^{\mathrm{jet}} > 100$ GeV after the b-tagging requirement (a) versus average number of collisions per bunch crossing and (b) versus the number of primary vertices in the event. The shaded band represents the bin-by-bin statistical uncertainty in simulation.

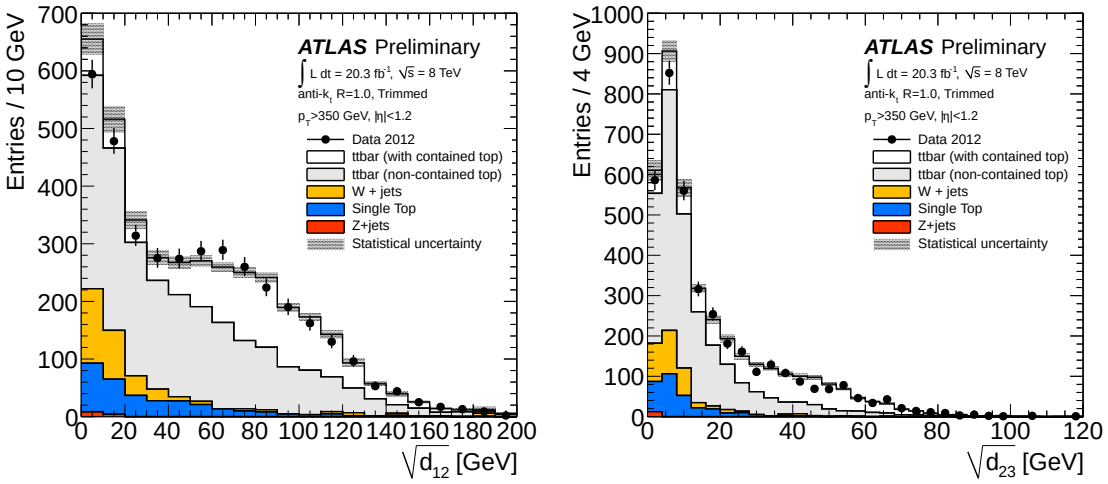

(a) (b)

Figure 4: Jet splitting scales for leading p_{T} anti-k_t trimmed jets with $R = 1.0$, $p_{\mathrm{T}} > 350$ GeV and $|\eta| < 1.2$ for events selected after a b-tag requirement, showing (a) the first splitting scale $\sqrt{d_{12}}$ and (b) the second splitting scale $\sqrt{d_{23}}$. The shaded band represents the bin-by-bin statistical uncertainty in simulation.

for events after the b-tagging requirement. After trimming, the background shape in the N-subjettiness ratios tends to mimic the shape of the signal distribution. This is due to the fact that, by construction, the trimming procedure preferentially keeps background events with jets exhibiting more "subjettiness".

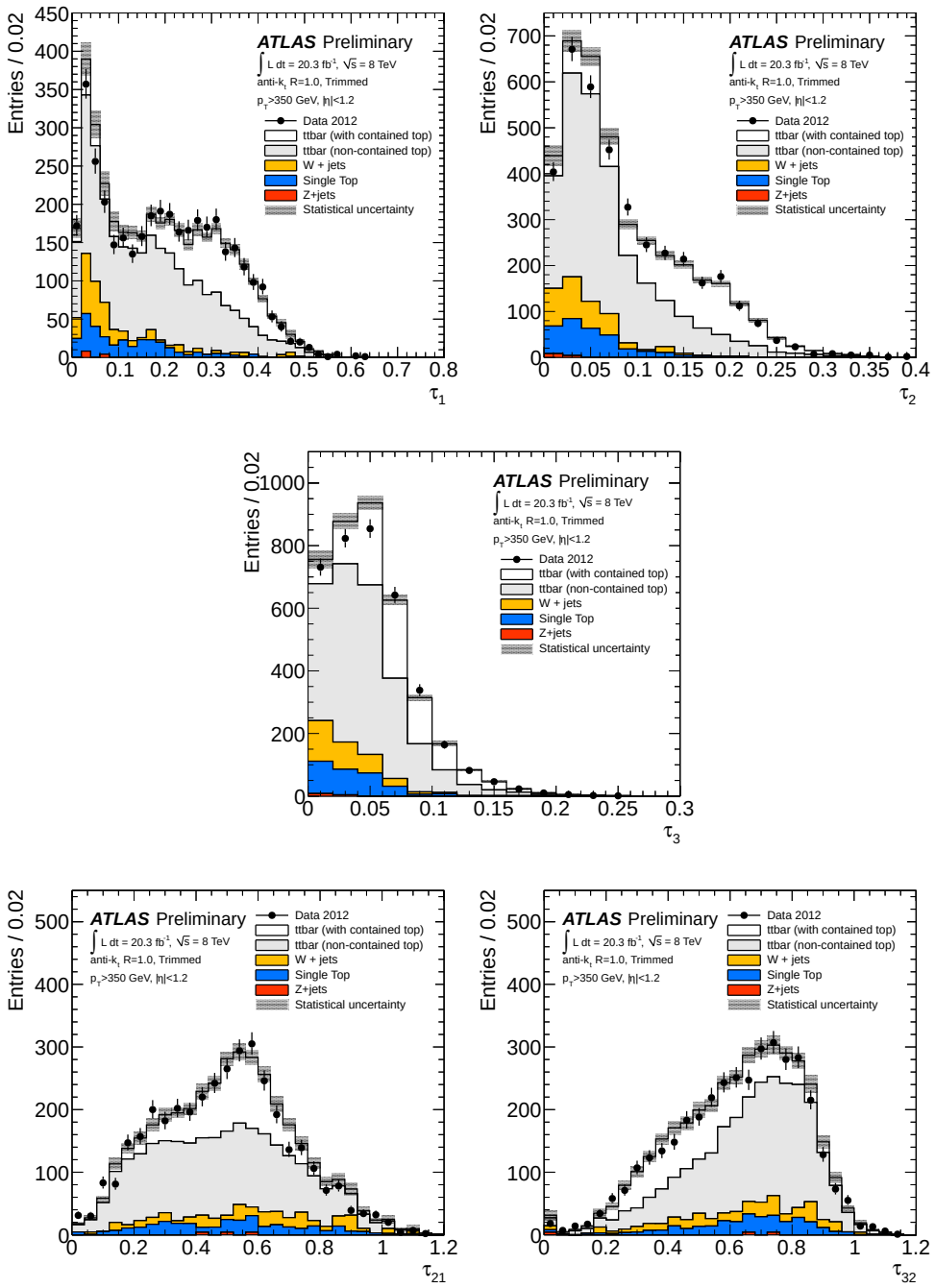

Figure 5: N-subjettiness for leading p_{T} anti-k_t trimmed jets with $R = 1.0$, $p_{\mathrm{T}} > 350$ GeV and $|\eta| < 1.2$ for events selected after a b-tagging requirement. The top and middle rows show the individual N-subjettiness variables τ_1, τ_2, and τ_3, while the bottom row shows the ratios τ_{21} and τ_{32}. The shaded band represents the bin-by-bin statistical uncertainty in simulation.

4.2 Composition of trimmed jets

As can be seen in Figure 2, jets containing boosted top quarks may still have a lower jet mass if one or more of the hadronic decay products falls outside the area of the jet. A comparison of different

classes of boosted top quarks can be made by studying the number of k_t subjets that are formed during the trimming procedure. Figure 6 shows the number of k_t subjets with $R_{\text{sub}} = 0.3$ after the b-tagging requirement in leading-p_{T} trimmed jets in two p_{T} regimes: $p_{\text{T}} > 350$ GeV and $p_{\text{T}} > 500$ GeV. The data are overestimated by the simulation for the $p_{\text{T}} > 500$ GeV case due to the p_{T} mismodeling as shown in Figure 1. Part of the discrepancy observed in the single subjet bin in both p_{T} regimes could be attributed to a large W+jets background normalization uncertainty (19% as shown in [36]).

The number of k_t subjets, and thus substructure in general, is highly dependent on the p_{T} of the top quark. There is a larger number of large-R jets with only two subjets at lower p_{T}, where one of the top decay products has fallen outside the area of the jet and most events fall under the "non-contained" category. As the jet p_{T} increases, the ratio of contained to non-contained top events in the two subjet bin increases due to the merging of k_t subjets that contain the decay products of the boosted top.

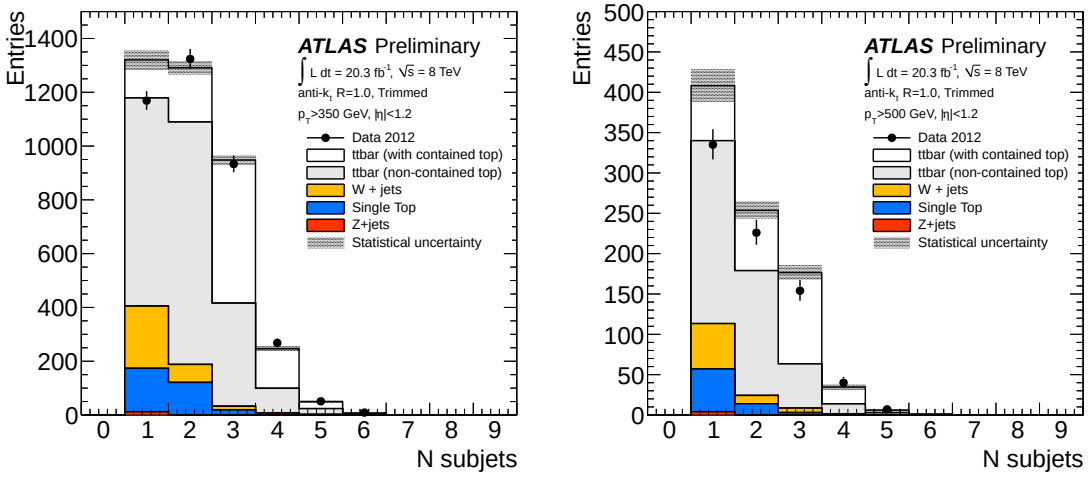

(a) $p_{\text{T}} > 350$ GeV

(b) $p_{\text{T}} > 500$ GeV

Figure 6: Number of k_t subjets after trimming on leading-p_{T} anti-k_t jets with $R = 1.0$ and $|\eta| < 1.2$, for two p_{T} regimes. See text for discussion related to the MC modeling of the data. The shaded band represents the bin-by-bin statistical uncertainty in simulation and does not include systematic uncertainties.

Figure 7 shows the leading-p_{T} trimmed jet mass for jets with $p_{\text{T}} > 350$ GeV, with one, two, three, and four or more k_t subjets after trimming. The majority of jets in the low-mass peak and the peak near $m^{\text{jet}} \approx m_W$ seen in Figure 2(a) have one and two k_t subjets, respectively, while most trimmed jets having mass near m_t have at least three subjets. Figure 8 shows the same mass distributions for jets with $p_{\text{T}} > 500$ GeV. In this p_{T} regime, there is a larger fraction of contained events near the top quark mass composed of only two subjets, signifying that the k_t-subjets are merging and that two of the three daughter particles from the top quark decay have been reconstructed as one subjet. The top mass shape is less well modeled in simulation in the two subjet bin in this p_{T} regime, but the shape is still within the statistical uncertainty of the data. It should also be noted that the mass scale uncertainty in this p_{T}-regime is estimated to be between 3-5%. Figure 9 demonstrates the p_{T}-dependence of this composition for simulated events that are required to satisfy the contained boosted top quark event requirement. The trimmed jets containing only one k_t-subjet at low mass, present in each of the p_{T}-regimes, are due to events where the jet containing the hadronic top quark decay products was not the leading-p_{T} jet.

Figure 10 shows splitting scale and N-subjettiness substructure variable distributions for leading-p_{T} trimmed jets with $p_{\text{T}} > 350$ GeV in simulated $t\bar{t}$ events satisfying the contained requirement. As in

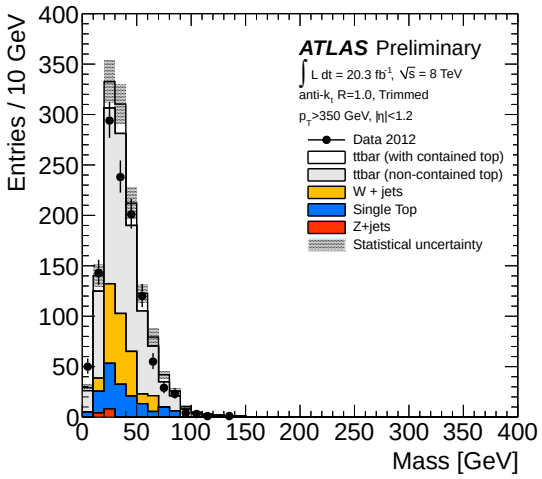

(a) $N_{subjets} = 1$

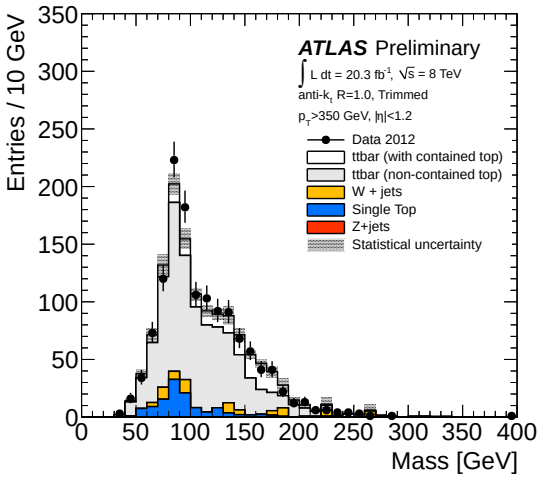

(b) $N_{subjets} = 2$

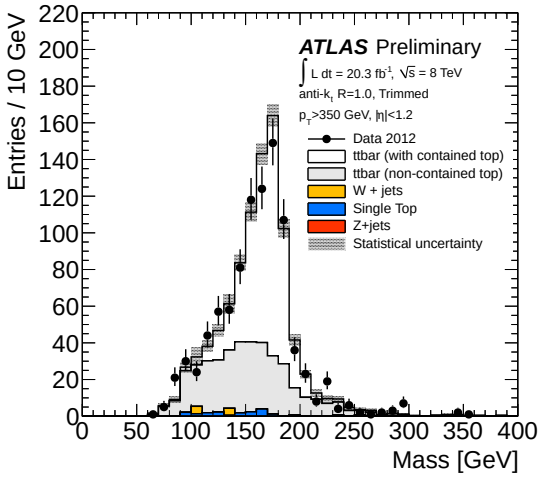

(c) $N_{subjets} = 3$

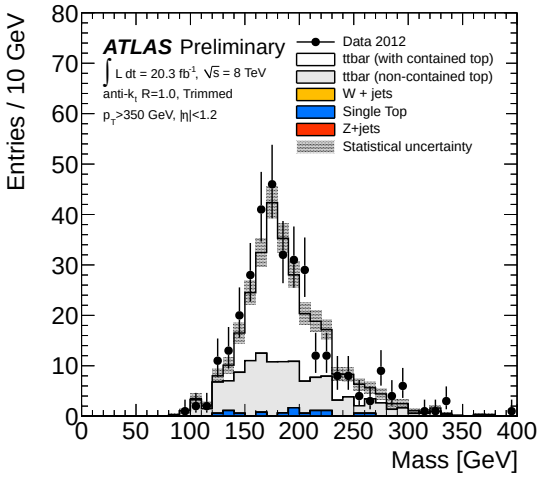

(d) $N_{subjets} \geq 4$

Figure 7: Jet mass for leading p_{T} anti-k_t trimmed jets with $R = 1.0$, $p_{\mathrm{T}} > 350$ GeV and $|\eta| < 1.2$ for events selected after a b-tagging requirement in bins of number of k_t subjets. The shaded band represents the bin-by-bin statistical uncertainty in simulation.

Figure 9, the trimmed jets with only one subjet represent events where the jet containing the boosted top quark was not the leading-p_{T} jet. As expected, the first splitting scale $\sqrt{d_{12}}$ separates trimmed jets with only one subjet from those which have a value $\sqrt{d_{12}} \approx m_W$. Trimmed jets with only two subjets have much lower values of the second splitting scale, $\sqrt{d_{23}}$, while jets with three or more subjets have a value of $\sqrt{d_{23}} \approx m_W/2$. For the first N-subjettiness ratio, τ_{21}, the separation between "signal"-like trimmed jets and a background composed of trimmed jets with only one subjet is largest for the signal jets composed of exactly two subjets. The separation power degrades with the addition of more subjets. This is expected by construction of the N-subjettiness algorithm. It is a similar case for τ_{32}, where the most "signal"-like trimmed jets have exactly three subjets.

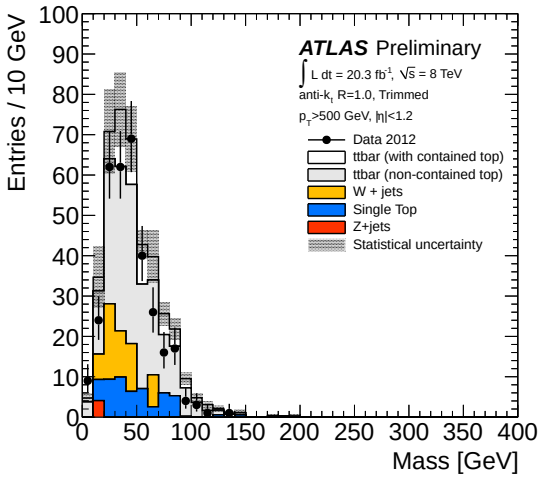

(a) $N_{subjets} = 1$

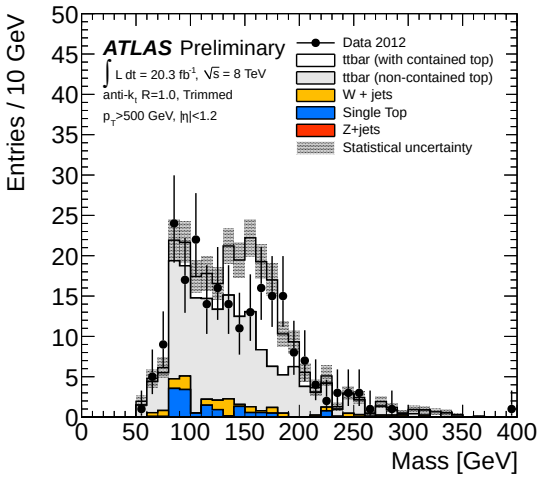

(b) $N_{subjets} = 2$

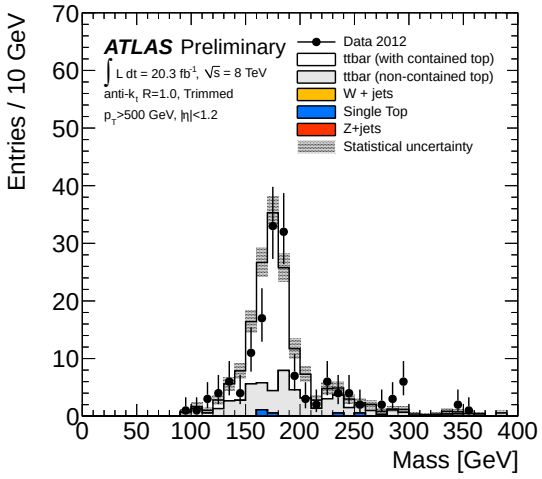

(c) $N_{subjets} = 3$

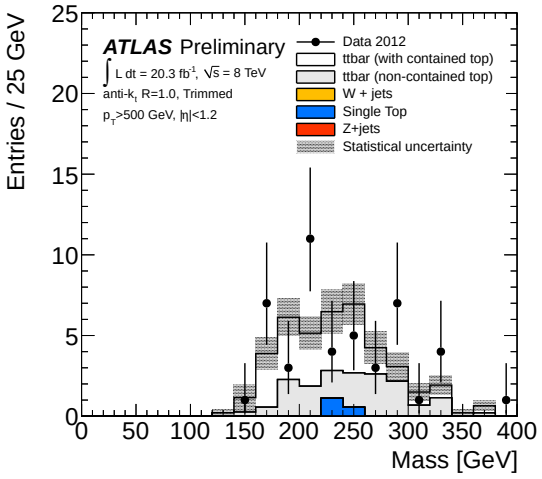

(d) $N_{subjets} \geq 4$

Figure 8: Jet mass for leading p_{T} anti-k_t trimmed jets with $R = 1.0$, $p_{\mathrm{T}} > 500$ GeV and $|\eta| < 1.2$ for events selected after a b-tagging requirement in bins of number of k_t subjets. The shaded band represents the bin-by-bin statistical uncertainty in simulation.

5 HEPTopTagger calibration and performance

5.1 Calibration of the HEPTopTagger

In the HEPTopTagger, cuts are applied on invariant mass ratios of subjet combinations and the top quark candidate mass is required to be within a certain mass interval. The calibration of the subjet energies and directions ensures good signal efficiency and background rejection and a good reconstruction of the top quark momentum vector.

Before calibrating the subjets, energy depositions that originate from pile-up are removed to a large extent by applying an area correction [44] to each jet [45]. In this correction, the product $\rho \times A_{\mathrm{T}}$ is subtracted from the jet p_{T}, in which ρ is the median p_{T} density of the event and A_{T} is the transverse

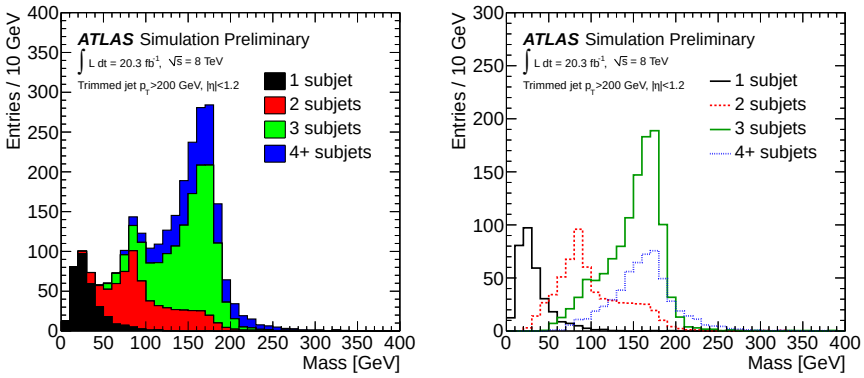

(a) (b)

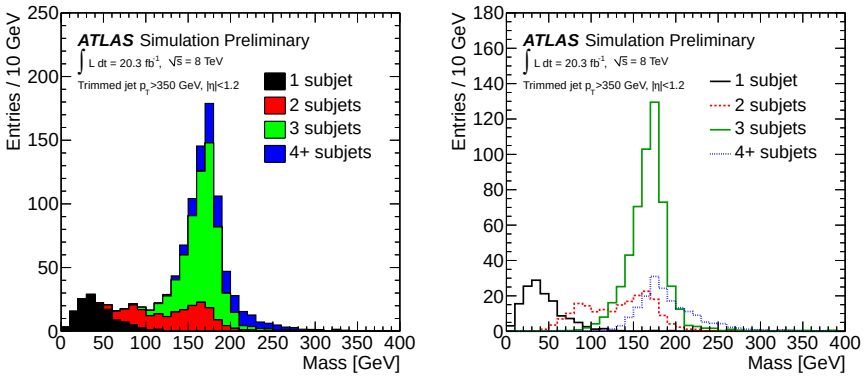

(c) (d)

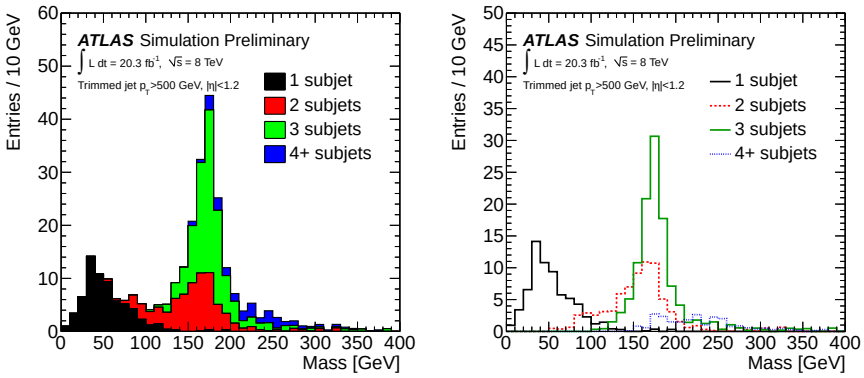

(e) (f)

Figure 9: Jet mass for leading p_{T} anti-k_t trimmed jets with $R = 1.0$ for $p_{\mathrm{T}} > 200$ GeV (top row), $p_{\mathrm{T}} > 350$ GeV (middle row) and $p_{\mathrm{T}} > 500$ GeV (bottom row), in simulated $t\bar{t}$ events with a contained boosted top at the truth level (all three daughter quarks q_i satisfy $\Delta R(q_i, t) < 1.0$). The left column shows the four subjet categories stacked, while the right column overlays these categories.

component of the jet area which is evaluated using ghost association [46]. The median p_{T} density is

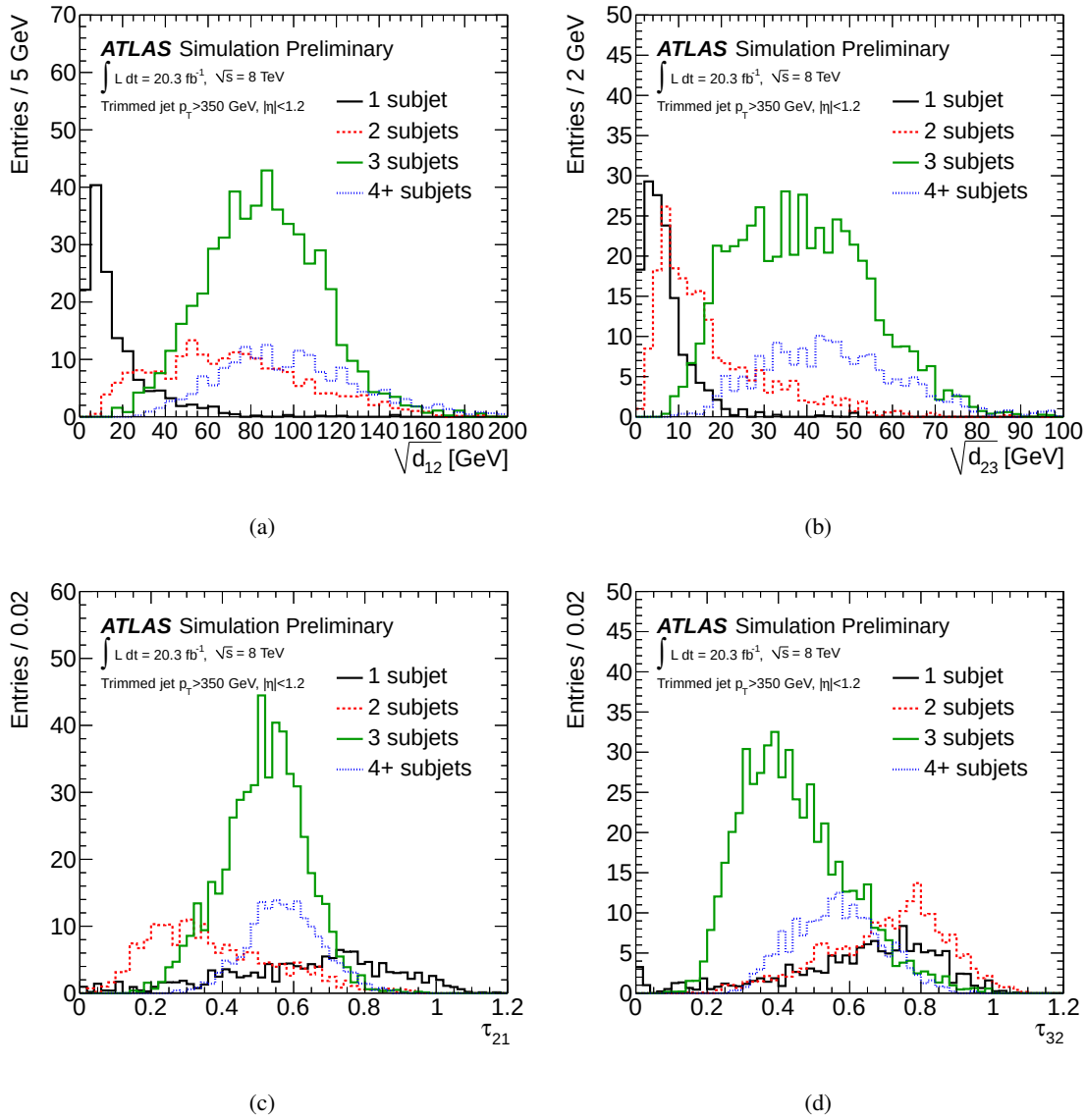

Figure 10: Distributions overlaid in bins of number of subjets for (a) the first splitting scale $\sqrt{d_{12}}$, (b) the second splitting scale $\sqrt{d_{23}}$, (c) N-subjettiness τ_{21}, and (d) N-subjettiness τ_{32}, in simulated $t\bar{t}$ events with a contained boosted top quark at the truth level (all three daughter quarks q_i satisfy $\Delta R(q_i, t)$ <1.0).

defined as

$$\rho = \text{median}\left\{p_{\text{T},i}^{\text{jet}}/A_i^{\text{jet}}\right\} \tag{3}$$

in which the index i enumerates the jets found when clustering the event with the k_t algorithm with $R = 0.4$ and requiring positive jet energy but no minimal jet p_{T}.

The pile-up-corrected jets are calibrated using a simulation of the calorimeter jet response by comparing the energy and pseudorapidity of a truth level particle jet to that of a matching calorimeter cluster jet [15, 47]. To be able to provide calibrations for the filtering step with its dynamic distance parameter R_{filt}, the calibration constants are derived for jets with $R = 0.2, 0.25, \ldots, 0.5$ and constants are used that correspond to R_{filt} or the next largest R if R_{filt} is not in the list of calibrated distance parameters. In the final exclusive clustering to three subjets, a radius is calculated for each exclusive subjet from the

distance of the constituents to the jet axis, and the corresponding calibration is used. Varying this radius by factors 2 and 0.5 has a negligible impact on the observed top quark candidate kinematics and a small impact on the substructure variables used to apply kinematic cuts.

The jet energy correction for C/A jets with $R = 0.4$ for $0 < \eta < 0.1$ amounts to +33% at $p_{\mathrm{T}} = 20$ GeV and +3% for $p_{\mathrm{T}} > 500$ GeV. The mean reconstructed p_{T} of the calibrated jet matches the p_{T} of the particle jet within less than 3% for all energies and pseudorapidities. For C/A $R = 0.2$ jets this closure is 4% at $p_{\mathrm{T}} = 20$ GeV and 2% or better for higher p_{T}.

5.2 HEPTopTagger performance with 2012 data

In this section distributions of the reconstructed top candidate mass, the tagger internal substructure variables and the pile-up stability using the top quark-enriched sample are shown. For the performance figures in this section the default settings described in Table 1 are used.

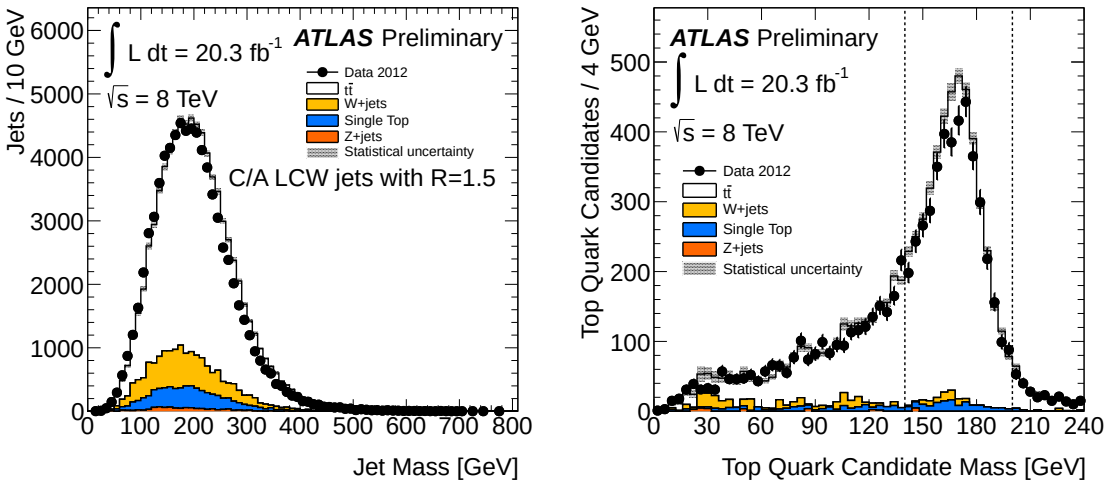

(a) (b)

Figure 11: Comparison between data and simulation for an event sample enriched in boosted top quarks. (a) Mass distribution for C/A jets with $R = 1.5$ before running the HEPTopTagger. (b) Mass distribution of the HEPTopTagger top quark candidate with $p_{\mathrm{T}} > 200$ GeV.

Figure 11 shows the mass distributions of (a) C/A $R = 1.5$ jets before running the HEPTopTagger and (b) HEPTopTagger top quark candidates. The jets and the top candidates are required to have $p_{\mathrm{T}} > 200$ GeV. The C/A jets are built from locally weighted clusters and not calibrated to the truth level. There is also no jet areas pile-up correction applied to these large-R jets. The large-R jet mass exhibits a broad peak with a maximum at 180 GeV. The distribution predicted by the simulation is shifted towards higher masses. Between 200 and 350 GeV the shift is approximately 10 GeV, which corresponds to a relative change of 5% at a mass of 200 GeV. This difference to the observed mass is within the typical simulation uncertainty found for large-R jets [15]. The HEPTopTagger candidate mass shows a peak at the top quark mass that falls rapidly towards larger masses. The tail towards lower masses results from cases where not all energy associated with the top quark decay is recovered. These losses occur in the filtering and when not all decay products are contained in the large-R jet. The effect on the mass distribution of tightening and loosening the filtering was shown in Ref. [15]. The top candidate mass is well described by simulation. The HEPTopTagger increases the purity from 86% $t\bar{t}$ and single-top-quark

processes before tagging to 98% in the candidate mass window $140 < m_t < 200$ GeV. The number of top quark candidates reconstructed in this mass window in the data is 4210.

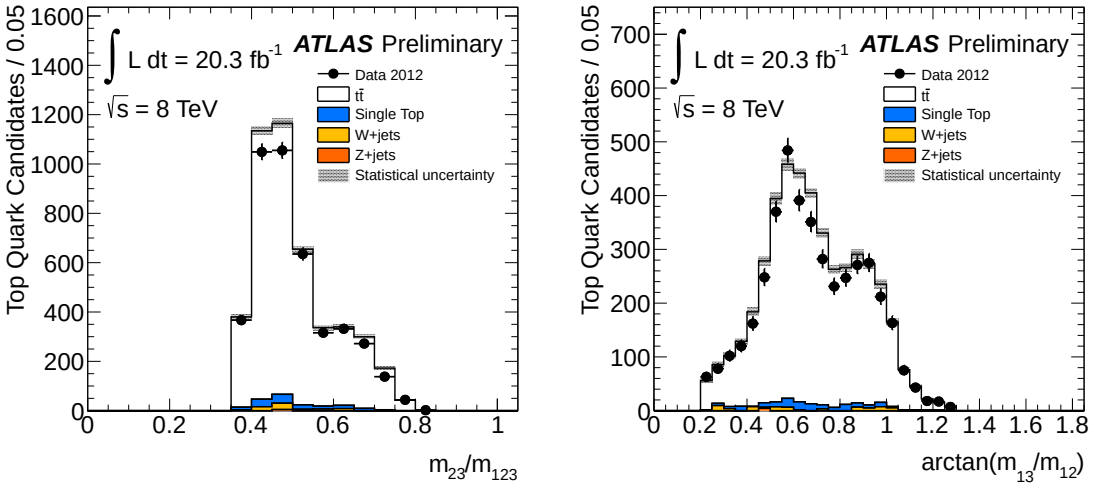

(a) (b)

Figure 12: HEPTopTagger substructure variables for top quark candidates. (a) The subjet invariant mass ratio m_{23}/m_{123}. (b) The quantity $\arctan(m_{13}/m_{12})$.

Distributions of substructure variables used inside the HEPTopTagger are shown in Figure 12 for the top quark candidates. These variables are invariant mass ratios of combinations of the three (exclusive) subjets that together form the top quark candidate. For example, the variable m_{23} is the invariant mass of the subleading p_{T} and the sub-subleading p_{T} subjet, and the variable m_{123} is the mass of the top quark candidate. The ratio m_{23}/m_{123} displayed in panel (a) shows a peak at m_W/m_t. This indicates that in most of the cases the leading p_{T} subjet corresponds to the b quark. The distribution is well described by the simulation. The same is true for the quantity $\arctan(m_{13}/m_{12})$ in panel (b).

Figure 13 shows the reconstructed top candidate mass for different pile-up conditions. The average candidate mass in the window $140 < m_t < 200$ GeV is plotted as a function of the average number of interactions per bunch-crossing μ in panel (a) and as a function of the number of reconstructed primary vertices N_{PV} in (b). The μ and N_{PV} intervals are chosen such that each average mass is calculated from at least 100 entries. Within the statistical uncertainty of the average mass of approximately ± 1 GeV, the reconstructed top quark mass is not affected by pile-up energy in the full accessible range up to $\mu = 31$ and $N_{\mathrm{PV}} = 19$. This is also seen for the generated semileptonic $t\bar{t}$ events that have been passed through a full ATLAS detector simulation under the same pile-up conditions. The numerical value of the reconstructed top quark mass depends on the choice of the mass window and is well predicted by the simulation.

6 Boosted top tagging performance

The substructure techniques presented here are used in LHC top quark physics analyses to extend the sensitivity to new physics scenarios. Searching for a resonance in the $t\bar{t}$ invariant mass spectrum has yielded an exclusion limit on the mass of a hypothetical leptophobic Z' boson of 1.74 TeV [18, 48–50].

The boosted top quark tagging efficiency and the rejection of jets arising from light quarks or gluons are determined from simulation. In order to study a sample of high-p_{T} top quarks, a Z' sample with

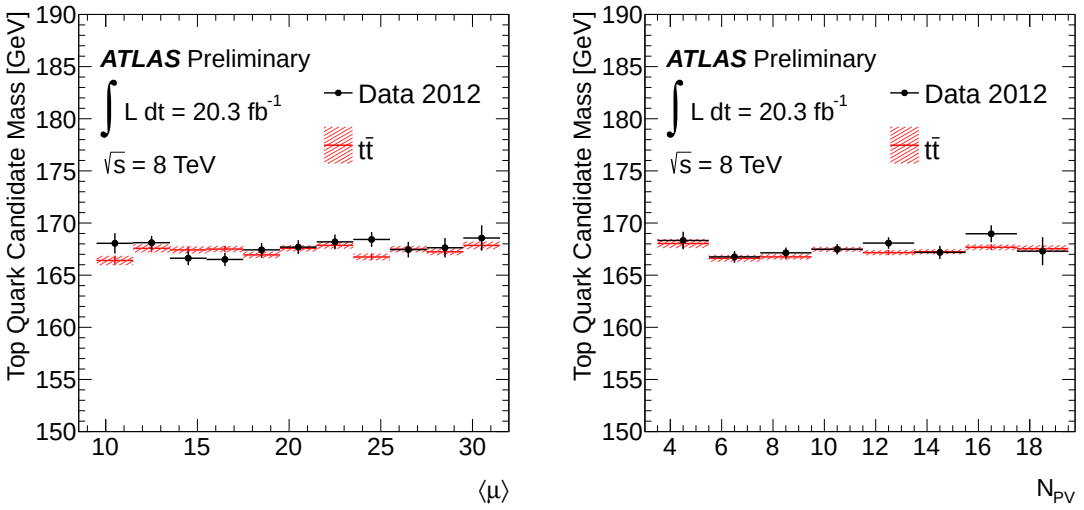

(a) (b)

Figure 13: HEPTopTagger top candidate mass as a function of (a) the average number of interactions per bunch-crossing μ and (b) the number of reconstructed primary vertices in the event. The mass is defined as the average mass in the window $140 < m_t < 200$ GeV and the error bar corresponds to the statistical uncertainty of the average mass. Also shown are predictions for semileptonic $t\bar{t}$ events that have been passed through a full ATLAS detector simulation.

$m_{Z'} = 1.75$ TeV is used, where the Z' bosons decay exclusively to $t\bar{t}$ in the semi-leptonic channel. To estimate the background rejection, an inclusive jet sample is used, where the leading anti-k_t $R = 0.6$ particle level jet p_{T} ranges from 500 to 1000 GeV.

Samples of truth level particle jets are defined for signal and background by requiring at least one C/A $R = 1.2$ jet and at least one trimmed anti-k_t $R = 1.0$ jet, both with $p_{\mathrm{T}} > 150$ GeV and $|\eta| < 1.2$. For the signal, the truth level requirements include a hadronically decaying top quark with $p_{\mathrm{T}} > 150$ GeV and $|\eta| < 1.2$ within $\Delta R < 0.75 \times R$ of the leading p_{T} large-R jet of either type. At the reconstruction level, events are required to contain at least one C/A $R = 1.2$ jet and at least one trimmed anti-k_t $R = 1.0$ jet, both with $p_{\mathrm{T}} > 550$ GeV and $|\eta| < 1.2$. Both reconstructed large-R jets are required to be matched within $\Delta R < 0.75 \times R$ to the corresponding truth level particle jet of the same algorithm and R parameter. The reconstructed C/A and anti-k_t large-R jets are also required to be within $\Delta R < 0.75$ of one another to ensure that the performance of the different taggers is measured using input objects from the same top quark decay.

The shape of the reconstruction level large-R jet p_{T} distribution is shown in Figure 14 for signal and background. For the signal, the spectrum reflects the Jacobian peak structure of the top quark p_{T} distribution and peaks near $m_{Z'}/2$. The p_{T} of the C/A jets is greater on average than the p_{T} of geometrically matched trimmed anti-k_t jets.

Six tagging working points that are based on the substructure of trimmed anti-k_t $R = 1.0$ jets using the procedure described in Section 4 are studied. The definitions of the working points are (in order of increasing background rejection):

- substructure tagger I: $\sqrt{d_{12}} > 40$ GeV (labeled '$\sqrt{d_{12}}$ tagger I' in Figure 15)
- substructure tagger II: trimmed anti-k_t $R = 1.0$ mass $m^{\mathrm{jet}} > 100$ GeV (labeled 'm^{jet} tagger II')
- substructure tagger III: $m^{\mathrm{jet}} > 100$ GeV, $\sqrt{d_{12}} > 40$ GeV (labeled 'm^{jet} & $\sqrt{d_{12}}$ tagger III')

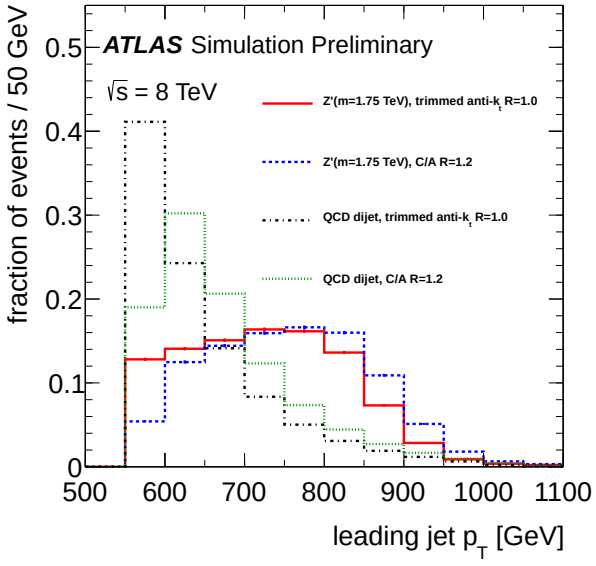

Figure 14: The large-R jet p_{T} spectra for signal ($Z' \to t\bar{t}$) and background (inclusive jets) that are used for the tagging comparison.

- substructure tagger IV: $m^{\mathrm{jet}} > 100$ GeV, $\sqrt{d_{12}} > 40$ GeV, $\sqrt{d_{23}} > 10$ GeV (labeled 'm^{jet} & $\sqrt{d_{12}}$ & $\sqrt{d_{12}}$ tagger IV')
- substructure tagger V: $m^{\mathrm{jet}} > 100$ GeV, $\sqrt{d_{12}} > 40$ GeV, $\sqrt{d_{23}} > 20$ GeV (labeled 'm^{jet} & $\sqrt{d_{12}}$ & $\sqrt{d_{12}}$ tagger V')
- substructure tagger VI: $\sqrt{d_{12}} > 40$ GeV, $0.4 < \tau_{21} < 0.9$, $\tau_{32} < 0.65$ (labeled '$\sqrt{d_{12}}$ & N-subjettiness tagger VI')

Tagger III working point was used in searches for $t\bar{t}$ resonances in the lepton+jets channel [36, 50]. The others are compared to study the performance of different combinations of substructure variables.

The HEPTopTagger is compared for three different sets of parameters specified in Table 1, where the inputs to the HEPTopTagger are C/A jets with $R = 1.2$. The distance parameter was lowered from the nominal 1.5 for which the HEPTopTagger was designed and optimized because of the large p_{T} of the top quarks under study, which leads to a collimation of the decay products to a smaller cone, and to make the radius parameter more similar to the one used for the trimmed jets.

Figure 15 shows a comparison of the efficiency ε for tagging large-R jets that contain a top quark and the rejection of large-R jets originating from hard light quarks or gluons. The rejection is defined as the inverse of the efficiency for tagging a light quark or gluon jet from an inclusive jet event. The best rejection of all studied taggers is obtained with the HEPTopTagger when using the tight settings, which, however, also results in the smallest efficiency. Loosening the HEPTopTagger parameters improves the efficiency at a cost in rejection. The performances obtained from the default and loose parameters differ only slightly.

The substructure tagger III, which has been used in $t\bar{t}$ resonance searches in the semileptonic channel, has a high efficiency and a small rejection. Such a working point is typically used in analyses in which the background has already been reduced by measures not related to jet substructure, such as the requirement of a final state lepton.

Tagger I is tagger III without the requirement on the trimmed large-R jet mass and yields a higher

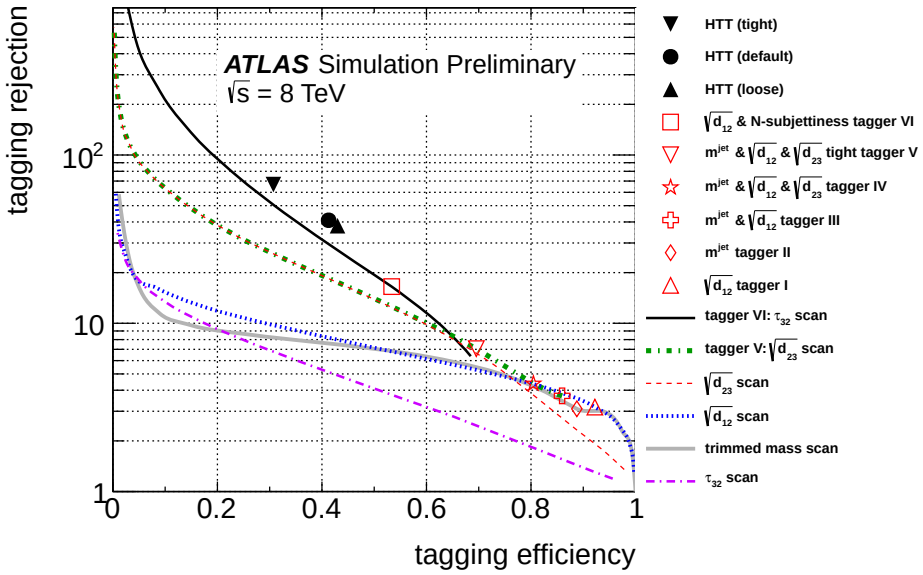

Figure 15: Comparison of the simulated large-R top jet tagging efficiency and large-R light quark/gluon jet rejection (defined as the inverse of the fake rate) of different taggers. The top jets originate from the decay of a Z' boson of mass 1.75 TeV and the jet p_{T} is required to be greater than 550 GeV. All substructure taggers and scans use trimmed anti-k_t $R = 1.0$ jets. The HEPTopTagger (points labeled 'HTT') uses Cambridge–Aachen $R = 1.2$ jets that are geometrically matched to the anti-k_t jets.

efficiency but worse rejection. The cut on $\sqrt{d_{12}}$ has been varied from the nominal 40 GeV for tagger I, resulting in the continuous curve labeled '$\sqrt{d_{12}}$ scan', which crosses the points for taggers III and IV. This indicates that, for the signal and background large-R jets under study here, the mass cut can be dropped from tagger III without compromising its performance. Adding a cut $\sqrt{d_{23}} > 10$ GeV (as in tagger IV) also does not help in separating signal from background. A larger cut value of 20 GeV in combination with the mass cut, however, increases the rejection as can be seen from the position of the tagger V point in relation to the curve. The variation of the m^{jet} cut in tagger II ('trimmed mass scan') gives a performance very similar to the one from the $\sqrt{d_{12}}$ cut, indicating that the two variables are strongly correlated.

We have also investigated the impact of a standalone cut on $\sqrt{d_{23}}$. The performance that results from varying the minimal required $\sqrt{d_{23}}$ ('$\sqrt{d_{23}}$ scan') offers better rejection than a cut on $\sqrt{d_{12}}$ for $\varepsilon \lesssim 75\%$, almost reaching that of tagger V which uses a combination of cuts on $\sqrt{d_{23}}$, $\sqrt{d_{12}}$, and the mass, suggesting that the latter two cuts can be dropped at minimal expense. The $\sqrt{d_{23}}$ cut in tagger V has been varied while keeping the other cuts fixed ('sub. V: $\sqrt{d_{23}}$ scan'), resulting in a performance which differs from that of $\sqrt{d_{23}}$ only for $\varepsilon \gtrsim 70\%$ where it gives better rejection. Variations of the other cuts in tagger V (one at a time, fixing the other cut-offs to their nominal values) do not improve the performance compared to the $\sqrt{d_{23}}$ variation.

A standalone cut on the N-subjettiness variable τ_{32} ('τ_{32} scan') yields a significantly worse performance than cuts on splitting scales. Combining N-subjettiness and splitting scale information (tagger VI), however, gives the best performance of all substructure variable based taggers for $\varepsilon \lesssim 60\%$. By varying the τ_{32} cut in tagger VI ('sub. VI: τ_{32} scan'), rejections of $\approx 75\%$ (70%) of those of the HEPTopTagger can be achieved for $\varepsilon \approx 40\%$ (30%).

For the present study, the performance of taggers based on substructure variables is driven by cuts

on splitting scales. For $\varepsilon \gtrsim 75\%$, a standalone cut on the first splitting scale $\sqrt{d_{12}}$ gives the best performance. At lower efficiencies, the second splitting scale $\sqrt{d_{23}}$ is the variable that in a standalone cut best separates signal from background. Adding N-subjettiness information increases the performance, whereas an additional cut on the trimmed large-R jet mass does not help significantly.

The studied substructure variable taggers achieve higher efficiencies than the HEPTopTagger. Compared at the same efficiency, however, they yield a smaller rejection, making the HEPTopTagger the tagger of choice for analyses in which the multijet background is large. Finding the best performance of the substructure taggers that are based on several variables requires a multi-dimensional variation of the cut values.

The top quark taggers presented here provide a broad spectrum of working points, and the best choice for any particular analysis depends on the needed efficiency and rejection, which are sensitive to the event topology, main background(s) and kinematic phase space.

7 Conclusions

Top quark tagging methods have been studied using the ATLAS data recorded in 2012. The semi-leptonic $t\bar{t}$ decay mode in which one W boson decays into a neutrino and a muon was chosen to select a sample of $t\bar{t}$ pairs which has been used to study the reconstruction of hadronically decaying boosted top quarks.

The optimal configuration for the anti-k_t algorithm with $R = 1.0$ implements the trimming parameters $f_{\text{cut}} = 0.05$ and $R_{\text{sub}} = 0.3$, and the substructure of leading p_{T} jets in the 2012 data sample enriched in semi-leptonic $t\bar{t}$ events is well modeled in simulation. Taking advantage of the k_t subjets built during the trimming procedure, it has been shown that as the top quark p_{T} increases, large-R jets are more likely to be composed of only two subjets, indicating that individual jets with smaller distance parameters, limited by detector resolution, would not be resolvable in top reconstruction.

The HEPTopTagger has been demonstrated to be a robust and versatile tool to tag hadronically decaying top quarks in the presence of the underlying event and pile-up using jet grooming and substructure techniques. The reconstructed top quark mass and the HEPTopTagger internal substructure variables are well described by simulation. The algorithm performance (top tagging efficiency versus light quark and gluon rejection) has been shown for several working points and can be optimized for a given analysis by varying the algorithm parameters.

The top quark mass reconstructed with the HEPTopTagger and by using the mass of trimmed anti-k_t $R = 1.0$ jets is stable with respect to the average number of interactions per bunch-crossing and the number of reconstructed vertices, both of which have increased significantly with respect to 2011 data because of the higher instantaneous LHC luminosity in 2012.

The top quark finding efficiency and background rejection of different tagging approaches, which in addition to the dedicated top-tagging algorithm HEPTopTagger also includes selection on k_t splitting scales and N-subjettiness of trimmed large-R jets, have been compared in simulation for a broad range of working points. While the HEPTopTagger has been designed to provide high rejection, the substructure information of trimmed jets may be used for analyses in which higher efficiency is required. For each type of tagger, efficiency and rejection can be tuned, where the optimal choice depends on the selection and event topology of a particular analysis.

References

[1] J. M. Butterworth et al., *Jet substructure as a new Higgs search channel at the LHC*, Phys. Rev. Lett. **100** (2008) 242001, arXiv:0802.2470 [hep-ph].

[2] S. D. Ellis, C. K. Vermilion, and J. R. Walsh, *Techniques for improved heavy particle searches with jet substructure*, Phys. Rev. **D 80** (2009) 051501, arXiv:0903.5081 [hep-ph].

[3] D. Krohn, J. Thaler, and L.-T. Wang, *Jet Trimming*, JHEP **02** (2010) 084, arXiv:0912.1342 [hep-ph].

[4] T. Plehn, G. P. Salam, and M. Spannowsky, *Fat Jets for a Light Higgs*, Phys. Rev. Lett. **104** (2010) 111801, arXiv:0910.5472 [hep-ph].

[5] T. Plehn et al., *Stop Reconstruction with Tagged Tops*, JHEP **10** (2010) 078, arXiv:1006.2833 [hep-ph].

[6] W. Lampl et al., *Calorimeter clustering algorithms: description and performance*, ATL-LARG-PUB-2008-002. http://cdsweb.cern.ch/record/1099735.

[7] S. Catani et al., *New clustering algorithm for multi-jet cross-sections in e^+e^- annihilation*, Phys. Lett. **B 269** (1991) 432.

[8] S. D. Ellis and D. E. Soper, *Successive combination jet algorithm for hadron collisions*, Phys. Rev. **D 48** (1993) 3160, arXiv:hep-ph/9305266 [hep-ph].

[9] S. Catani et al., *Longitudinally invariant $k_\perp$ clustering algorithms for hadron hadron collisions*, Nucl. Phys. **B 406** (1993) 187.

[10] Y. L. Dokshitzer et al., *Better jet clustering algorithms*, JHEP **08** (1997) 001, arXiv:hep-ph/9707323 [hep-ph].

[11] M. Wobisch and T. Wengler, *Hadronization corrections to jet cross sections in deep- inelastic scattering*, arXiv:hep-ph/9907280 [hep-ph].

[12] M. Cacciari, G. P. Salam, and G. Soyez, *The anti-k_t jet clustering algorithm*, JHEP **04** (2008) 063, arXiv:0802.1189 [hep-ph].

[13] M. Cacciari and G. P. Salam, *Dispelling the N^3 myth for the k_t jet-finder*, Phys. Lett. **B 641** (2006) 57, arXiv:hep-ph/0512210 [hep-ph].

[14] M. Cacciari, G. P. Salam, and G. Soyez, *FastJet User Manual*, Eur. Phys. J. **C 72** (2012) 1896, arXiv:1111.6097 [hep-ph].

[15] ATLAS Collaboration, *Performance of jet substructure techniques for large-R jets in proton-proton collisions at $\sqrt{s} = 7$ TeV using the ATLAS detector*, submitted to JHEP (2013) , arXiv:1306.4945 [hep-ex].

[16] J. Thaler and K. Van Tilburg, *Identifying Boosted Objects with N-subjettiness*, JHEP **03** (2011) 015, arXiv:1011.2268 [hep-ph].

[17] J. Thaler and K. Van Tilburg, *Maximizing Boosted Top Identification by Minimizing N-subjettiness*, JHEP **02** (2012) 093, arXiv:1108.2701 [hep-ph].

[18] ATLAS Collaboration, *Search for resonances decaying into top-quark pairs using fully hadronic decays in pp collisions with ATLAS at $\sqrt{s} = 7$ TeV*, JHEP **01** (2013) 116, arXiv:1211.2202 [hep-ex].

[19] ATLAS Collaboration, *The ATLAS Experiment at the CERN Large Hadron Collider*, JINST **3** (2008) S08003.

[20] ATLAS Collaboration, *Improved luminosity determination in pp collisions at $\sqrt{s} = 7$ TeV using the ATLAS detector at the LHC*, submitted to Eur. Phys. J. (2013) , arXiv:1302.4393 [hep-ex].

[21] P. Nason, *A New method for combining NLO QCD with shower Monte Carlo algorithms*, JHEP **11** (2004) 040, arXiv:hep-ph/0409146 [hep-ph].

[22] S. Frixione, P. Nason, and C. Oleari, *Matching NLO QCD computations with Parton Shower simulations: the POWHEG method*, JHEP **11** (2007) 070, arXiv:0709.2092 [hep-ph].

[23] S. Alioli et al., *Jet pair production in POWHEG*, JHEP **04** (2011) 081, arXiv:1012.3380 [hep-ph].

[24] H.-L. Lai et al., *New parton distributions for collider physics*, Phys. Rev. **D 82** (2010) 074024, arXiv:1007.2241 [hep-ph].

[25] T. Sjostrand, S. Mrenna, and P. Z. Skands, *PYTHIA 6.4 Physics and Manual*, JHEP **0605** (2006) 026, arXiv:hep-ph/0603175 [hep-ph].

[26] J. Pumplin et al., *New generation of parton distributions with uncertainties from global QCD analysis*, JHEP **0207** (2002) 012, arXiv:hep-ph/0201195 [hep-ph].

[27] ATLAS Collaboration, *New ATLAS event generator tunes to 2010 data*, ATL-PHYS-PUB-2011-008. http://cdsweb.cern.ch/record/1345343.

[28] ATLAS Collaboration, *ATLAS tunes for Pythia6 and Pythia8 for MC11*, ATLAS-PHYS-PUB-2011-009. http://cdsweb.cern.ch/record/1363300.

[29] S. Frixione and B. R. Webber, *Matching NLO QCD computations and parton shower simulations*, JHEP **06** (2002) 029, arXiv:hep-ph/0204244 [hep-ph].

[30] S. Frixione, P. Nason, and B. R. Webber, *Matching NLO QCD and parton showers in heavy flavor production*, JHEP **0308** (2003) 007, arXiv:hep-ph/0305252 [hep-ph].

[31] G. Corcella et al., *HERWIG 6.5 release note*, arXiv:0210213 [hep-ph].

[32] J. M. Butterworth, J. R. Forshaw, and M. H. Seymour, *Multiparton interactions in photoproduction at HERA*, Z. Phys. C **72** (1996) 637, arXiv:9601371 [hep-ph].

[33] B. P. Kersevan and E. Richter-Was, *The Monte Carlo event generator AcerMC versions 2.0 to 3.8 with interfaces to PYTHIA 6.4, HERWIG 6.5 and ARIADNE 4.1*, Comp. Phys. Comm. **184** (2013) 919, arXiv:hep-ph/0405247 [hep-ph].

[34] ATLAS Collaboration, *Summary of ATLAS Pythia 8 tunes*, ATL-PHYS-PUB-2012-003. http://cdsweb.cern.ch/record/1474107.

[35] M. L. Mangano et al., *ALPGEN, a generator for hard multiparton processes in hadronic collisions*, JHEP **0307** (2003) 001, arXiv:hep-ph/0206293 [hep-ph].

[36] ATLAS Collaboration, *A search for $t\bar{t}$ resonances in lepton plus jets events with ATLAS using 14 fb^{-1} of proton-proton collisions at $\sqrt{s} = 8$ TeV*, ATLAS-CONF-2013-052. http://cdsweb.cern.ch/record/1543917.

[37] ATLAS Collaboration, *Measurement of the charge asymmetry in top quark pair production in pp collisions at $\sqrt{s} = 7$ TeV using the ATLAS detector*, Eur. Phys. J. **C 72** (2012) 2039, arXiv:1203.4211 [hep-ex].

[38] T. Sjostrand, S. Mrenna, and P. Z. Skands, *A Brief Introduction to PYTHIA 8.1*, Comput. Phys. Commun. **178** (2008) 852–867, arXiv:0710.3820 [hep-ph].

[39] A. Martin et al., *Parton distributions for the LHC*, Eur. Phys. J. **C 63** (2009) 189–285, arXiv:0901.0002 [hep-ph].

[40] GEANT4 Collaboration, *GEANT4: A simulation toolkit*, Nucl. Instrum. Meth. **A 506** (2003) 250.

[41] ATLAS Collaboration, *The ATLAS simulation infrastructure*, Eur. Phys. J. **C 70** (2010) 823, arXiv:1005.4568 [physics.ins-det].

[42] ATLAS Collaboration, *Selection of jets produced in proton-proton collisions with the ATLAS detector using 2011 data*, ATLAS-CONF-2012-020. http://cdsweb.cern.ch/record/1430034.

[43] ATLAS Collaboration, *Measurement of the b-tag efficiency in a sample of jets containing muons with 5 fb^{-1} of data from the ATLAS Detector*, ATLAS-CONF-2012-043. http://cdsweb.cern.ch/record/1435197.

[44] M. Cacciari and G. P. Salam, *Pileup subtraction using jet areas*, Phys. Lett. **B 659** (2008) 119, arXiv:0707.1378 [hep-ph].

[45] ATLAS Collaboration, *Pile-up subtraction and suppression for jets in ATLAS*, ATLAS-CONF-2013-083. http://cds.cern.ch/record/1570994.

[46] M. Cacciari, G. P. Salam, and G. Soyez, *The Catchment Area of Jets*, JHEP **04** (2008) 005, arXiv:0802.1188 [hep-ph].

[47] ATLAS Collaboration, *Jet energy measurement with the ATLAS detector in proton-proton collisions at $\sqrt{s} = 7$ TeV*, Eur. Phys. J. **C 73** (2013) 2304, arXiv:1112.6426 [hep-ex].

[48] CMS Collaboration, *Search for anomalous $t\bar{t}$ production in the highly-boosted all-hadronic final state*, JHEP **09** (2012) 029, arXiv:1204.2488 [hep-ex].

[49] CMS Collaboration, *Search for resonant $t\bar{t}$ production in lepton+jets events in pp collisions at $\sqrt{s} = 7$ TeV*, JHEP **12** (2012) 015, arXiv:1209.4397 [hep-ex].

[50] ATLAS Collaboration, *A search for $t\bar{t}$ resonances in the lepton plus jets final state with ATLAS using 4.7 fb^{-1} of pp collisions at $\sqrt{s} = 7$ TeV*, submitted to Phys. Rev. **D** (2013) , arXiv:1305.2756 [hep-ex].